^{13}C NMR Pattern of $Sc_3N@C_{68}$. Structural Assignment of the First Fullerene with Adjacent Pentagons

J. Ulises Reveles,[†] Thomas Heine,*[,‡] and Andreas M. Köster[†]

Departamento de Química, Cinvestav, Avenida Instituto Politécnico Nacional 2508 A.P. 14-740 México D.F. 07000, México, and Institut für Physikalische Chemie und Elektrochemie, TU Dresden, D-01062 Dresden, Germany

Received: April 21, 2005; In Final Form: June 20, 2005

$Sc_3N@C_{68}$ is assigned to isomer $Sc_3N@C_{68}$:6140 on the grounds of relative energies, geometrical data, and its ^{13}C NMR pattern. $Sc_3N@C_{68}$:6140 is an endohedral fullerene where each Sc atom is coordinated to the center of an equatorial pentalene unit. Static and dynamic computer simulations explain the different point groups observed in NMR and X-ray experiments. Computed and experimental ^{13}C NMR pattern are in close agreement except for one low-intensity signal. The competing isomer $Sc_3N@C_{68}$:6275 is found to be 409 kJ/mol less stable and shows a different ^{13}C NMR pattern.

I. Introduction

The encapsulation of the Sc_3N cluster into fullerene cages has created a new family of metallofullerenes with special structural and electronic properties. These fullerenes have been characterized by various methods, including mass, ^{13}C NMR, UV/vis, and Raman spectroscopies.[1−8] The first progress toward potential applications based on these new materials has been reported recently. For example, it has been shown that $Sc_3N@C_{80}$ is soluble in water,[9] and its successful functionalization[10] has been reported.

The special properties of this class of fullerenes is based on the transfer of up to six electrons from the endohedral Sc_3N moiety to the cage.[11] The resulting change of electronic structure of the carbon cage leads to stabilization of fullerenes which are usually highly reactive.[12−14] In all examples of these metallofullerenes, the ^{13}C NMR pattern, together with the mass spectrum, was the principal method for their characterization. Later, after the production of larger quantities, also X-ray experiments have been possible. The results of the X-ray analysis and those of the ^{13}C NMR measurements often disagree for the overall symmetry of the endohedral fullerenes, which has been explained with the high mobility of the endohedral molecule in the cage and the different time scales of vibrational spectroscopy and NMR experiments.

In particular, for $Sc_3N@C_{80}$, the encapsulated cluster is found to be highly mobile. First evidence for its nearly free rotation was found in the experimental ^{13}C NMR pattern. The spectrum reveals I_h symmetry, the same point group as for the empty icosahedral C_{80} cage.[1] Because the D_{3h} symmetry of the endohedral Sc_3N cluster would break the I_h symmetry, the experimental ^{13}C NMR pattern of $Sc_3N@C_{80}$ is only consistent with a nearly free rotation of Sc_3N, which averages out the lower symmetries.

However, on the short time scale infrared and Raman spectroscopy indicate C_3 and C_{3v} symmetries, depending on the orientation of Sc_3N with respect to the cage.[7] Recently, density functional based tight-binding (DFTB) Born−Oppenheimer molecular dynamics (BOMD) simulations confirmed the long-time ^{13}C NMR spectrum and showed that the flat D_{3h} Sc_3N unit rotates and tumbles with a very low barrier inside the C_{80} cage.[15] On a simulation time scale of 0.7 ns, the experimental ^{13}C NMR pattern was reproduced with an absolute error of less than 2 ppm, which is the expected intrinsic accuracy of such type of simulations.[16] On the other hand, Campanera et al. argued that the rotation of the Sc_3N moiety should be already hindered in slightly smaller $Sc_3N@C_{78}$, as different conformers show quite different relative energies in their gradient corrected density functional theory (DFT) calculations.[17]

$Sc_3N@C_{68}$ is another metallofullerene of this family, but with strong differences concerning the encapsulating cage. It is much smaller and contains adjacent pentagons that form pentalene like units. The identification of the structure of $Sc_3N@C_{68}$ is based on information gained by ^{13}C NMR measurements, theoretical chemistry, quantum chemical computation of relative energies[2] and on a recent X-ray study.[5] The ^{13}C NMR pattern contains 12 singlet peaks, 11 of full intensity and one of one-third intensity.[2] Graph theoretically, 6332 fullerene isomers are possible for C_{68}, but only 11 of them are consistent with the result of the ^{13}C NMR spectrum. From these 11 cages 10 possess D_3 symmetry and one has S_6 symmetry. Out of these 11 isomers, two—both of them D_3 cages—have the minimum number of three fused pentagons. The other relevant isomers contain more fused pentagons. The minimum number of pentagon adjacencies was one argument for the reduction of the set of possible isomer candidates from 11 to only 2. Indeed, the number of adjacent pentagons determines the stability of fullerenes. It has been shown that, as a rule of thumb, a fused pentagon is connected with an energy penalty of 70−90 kJ/mol for a fullerene cage.[18] This qualitative rule has been confirmed for the 11 D_3 and S_6 isomers of $Sc_3N@C_{68}$. DFTB calculations find the two isomers with three pentagon adjacencies, C_{68}:6140 and C_{68}:6275 in the spiral nomenclature,[19] to be the most stable.[2] C_{68}:6140 was found to be 120 kJ/mol more stable than C_{68}:6275. Within the same framework the expected charge transfer from the encapsulated cluster to the cage was modeled by adding two to six excess electrons to the empty cages. As a result isomer C_{68}^{6-}:6140 becomes increasingly favored over the 10 other isomers of the

[†] Cinvestav.
[‡] TU Dresden.

10.1021/jp052062n CCC: $30.25
Published on Web 07/22/2005

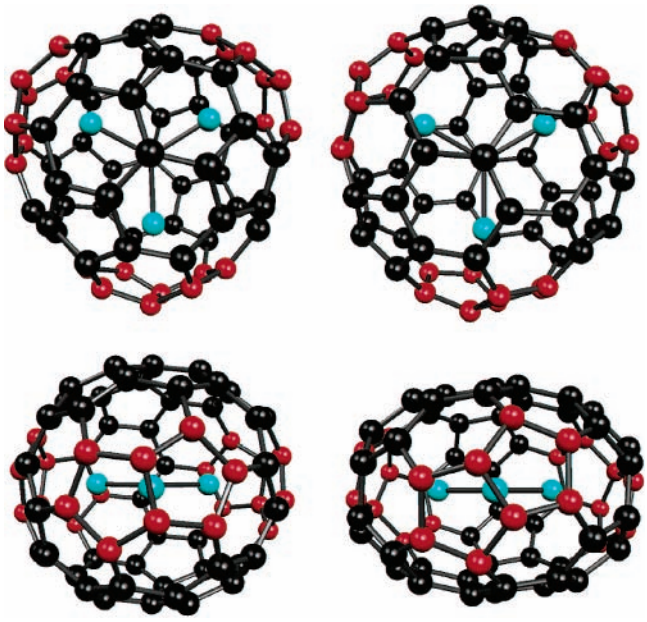

Figure 1. Optimized structures of $Sc_3N@C_{68}$:6140 (left) and $Sc_3N@C_{68}$:6275 (right).

set.[2] Thus, the structures of C_{68}:6140 and C_{68}:6275 match perfectly the necessities to incorporate the Sc_3N moiety. The C_3 axis is passing through the poles of the cages, and the three fused pentagons are located around their "equators" . Both, Sc atoms of the Sc_3N cluster and the pentalene units of the cage can be aligned to each other if common C_3 axes of cage and metal cluster are chosen (see Figure 1).

In this paper, we present first principle DFT calculations of the two isomers $Sc_3N@C_{68}$:6140 and $Sc_3N@C_{68}$:6275. On the basis of these calculations, we assign $Sc_3N@C_{68}$:6140 to the experimentally observed $Sc_3N@C_{68}$ isomer. The comparison of the calculated and measured geometry as well as the ^{13}C NMR pattern supports our assignment.

II. Computational Details

All calculations were performed using deMon software.[21,22] An auxiliary basis set[23] was used for the variational fitting of the Coulomb and exchange-correlation potential.[24] The numerical integration of the exchange-correlation energy and potential were performed on an adaptive grid.[25] Geometry optimizations and NMR computations have been carried out using the generalized gradient approximation (GGA) of Perdew, Burke, and Ernzerhof.[26] For geometry optimization and NMR calculations the DZVP[27] and IGLO-III[28] basis sets were employed, respectively. Microcanonical BOMD simulations (constant number of particles and energy, NVE) were performed at the density functional based tight-binding (DFTB) level[7,29] for 1 ns simulation time with a time step of 0.5 fs.

Molecular coordinates have been taken from previous work[2] and pre-optimized at the DFTB level. NMR snapshots along the MD trajectories have been computed with the same details as for the static computations but with the smaller IGLO-II basis set.[28] The minimum structures were fully optimized in delocalized internal coordinates without constraints using the RFO method and the BFGS update.[30] The ^{13}C NMR shifts are referred to C_{60} and then transformed to shifts with respect to TMS. The experimental signal of C_{60} was taken to be 142.68 ppm,[31] and the chemical shift δ of nucleus I is given as a function of the shielding constant σ by $\delta_I = \delta_{TMS}(C_{60}) + \sigma(C_{60}) - \sigma_I$.

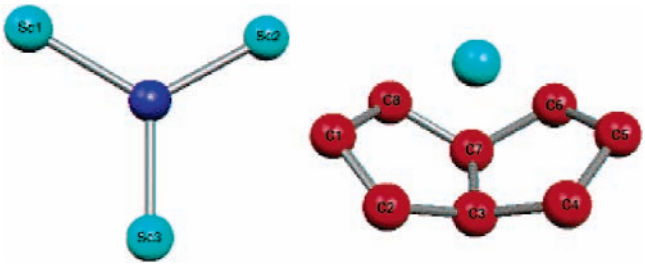

Figure 2. Labeling of Sc_3N scandiums and of pentalene carbons for geometry comparison in Tables 1 and 2.

III. Results and Discussion

A. Topology, Geometry, and Relative Energies. For C_{68}, it is topologically impossible to satisfy the isolated pentagon rule.[19,32,33] Only two out of the 6332 distinct C_{68} fullerene isomers have the lowest number of pentagon−pentagon adjacencies and are compatible with the experimental ^{13}C NMR pattern of 12 signals, 11 of full and one of one-third intensity.[2] In the original work,[2] it was only feasible to perform model computations of empty cages. Energetically, 68:6140 was reported to be the most stable isomer out of the 11 candidates which correspond to the experimental spectrum if they were discussed as neutral cages and di-, tetra-, and hexaanions. The second isomer, 68:6275, was found to be 120 kJ/mol less stable at the DFTB level. The electronic model of a charge transfer of six electrons from the encapsulated Sc_3N moiety to the cage was supported by an increase of the HOMO−LUMO gap when six excess electrons were added to 68:6140. In this work, we fully optimized both isomers of $Sc_3N@C_{68}$, and our GGA/DZVP computations favor isomer $Sc_3N@C_{68}$:6140 even more strongly, namely by 409 kJ/mol with respect to the $Sc_3N@C_{68}$:6275 isomer.[35]

Geometrically, 68:6140 is more spherical than 68:6275 and so are the corresponding metallofullerene isomers $Sc_3N@C_{68}$. It may appear that strong curvature is energetically unfavorable for fullerene cages, but indeed, aspherical fullerenes can be reasonably stable, as has been shown for the complete sets of larger fullerenes C_{118} and C_{120},[34] and this fact should be discarded as an argument in the discussion on stability. Another topological fact plays a more important role, namely that the three pentalene units are located around the equatorial belt, which lies in the plane perpendicular to the C_3 axis and through the center of the cage. Only in this topological arrangement the endohedral Sc_3N moiety can be placed in such way that each Sc atom faces a pentalene group without breaking its D_{3h} symmetry. In summary, both isomers have a topology which is perfectly suited to encapsulate the Sc_3N cluster.

Differences arise when the geometries are compared in detail. In Figure 2 and Table 1, our computed geometrical parameters of the endohedral moiety and of the pentalene units are compared with experimental X-ray data.[5] The computed Sc−C and Sc−N bond lengths of $Sc_3N@C_{68}$:6140 are in much closer agreement with the X-ray data than for $Sc_3N@C_{68}$:6275. In detail, the optimized $Sc_3N@C_{68}$:6140 bond lengths possess a mean absolute deviation from experiment of 2.7 pm. For the Sc−C bond lengths, the maximum deviation is 8.0 pm for the $Sc-C_7$ bond length, the next two largest deviations are 7.8 and 5.1 pm for the $Sc-C_6$ and $Sc-C_8$ bond lengths. The rest of the deviations are smaller than 3.6 pm. The maximum deviation in the N−Sc bond lengths is 3.5 pm. The reported Sc−C bond lengths are averaged for the three Sc atoms. The differences in the unconstrained optimized bond lengths are less than 1 pm. Also for the corresponding dihedral angles of the endohedral

TABLE 1: Experimental and Optimized Structural Parameters of $Sc_3N@C_{68}$ (bond lengths in Å and Angles in °)

		PBE/DZVP	
	expt[5]	$Sc_3N@C_{68}$:6140	$Sc_3N@C_{68}$:6275
$N-Sc_1$	2.022	1.997	2.034
$N-Sc_2$	1.974	1.995	2.031
$N-Sc_3$	1.961	1.996	2.033
$Sc-C_1$	2.43	2.44	2.53
$Sc-C_2$	2.39	2.39	2.48
$Sc-C_3$	2.28	2.31	2.36
$Sc-C_4$	2.35	2.35	2.35
$Sc-C_5$	2.40	2.44	2.53
$Sc-C_6$	2.31	2.39	2.48
$Sc-C_7$	2.23	2.31	2.36
$Sc-C_8$	2.30	2.35	2.35
Sc_1-N-Sc_2	130.3	120.0	119.9
Sc_1-N-Sc_3	113.8	120.0	119.9
Sc_2-N-Sc_3	115.9	120.0	120.1
$C_2C_3C_7C_4$	134.4	131.5	132.4

TABLE 2: Optimized Bond Lengths of the Pentalene Units of $Sc_3N@C_{68}$:6140 and the Corresponding Bare Cage C_{68}:6140 (in Å)

	$Sc_3N@C_{68}$	C_{68}
C_1-C_2/C_5-C_6	1.47	1.45
C_2-C_3/C_6-C_7	1.46	1.43
C_3-C_4/C_7-C_8	1.45	1.43
C_4-C_5/C_1-C_8	1.46	1.46
C_3-C_7	1.45	1.44

cluster only small differences (<0.1°) are found. For the $Sc_3N@C_{68}$:6275 isomer the optimized bond lengths possess a mean absolute deviation of 8.1 pm, about three times larger than for $Sc_3N@C_{68}$:6140! For the Sc−C bond length the maximum deviation is 17 pm for the $Sc-C_6$ bond length, the next two largest deviations are 13 pm for the $Sc-C_5$ and $Sc-C_7$ bond lengths, the rest of the deviations are smaller than 10 pm. The maximum deviation in the N−Sc bond length is 7.2 pm. Therefore, we can conclude that the unconstrained optimization of $Sc_3N@C_{68}$:6140 results in a D_3 symmetry which is in much closer agreement with the X-ray data. The reported experimental ScNSc bond angles, being strongly distorted from a C_3 axis, are neither compatible with experimental ^{13}C NMR data nor with our optimized minimum structures. In Table 2, the C−C bond lengths of the pentalene units of $Sc_3N@C_{68}$:6140 and its bare cage are compared. In the empty fullerene, the bond lengths of the pentalene units are on average 0.02 Å shorter than in $Sc_3N@C_{68}$, while the bond length alternation is higher in the bare cage. In particular, the bonds next to the bond connecting the two pentagons are shorter in the bare cage (1.43 Å) than in $Sc_3N@C_{68}$ (1.45−1.46 Å). These values indicate a partial electron transfer to the dipentalene units which stabilizes the local π system.

The direct coordination of Sc to the centers of the dipentalenes suggests that Sc_3N is bonded to C_{68} and forms a rigid structure and not, as in the case of $Sc_3N@C_{80}$, a cage including a nearly freely rotating cluster.[15] However, strong deviations between X-ray and optimized geometries suggest that dynamical effects may have caused an X-ray structure which is incompatible with the ^{13}C NMR experiment. Details will be discussed below, in the molecular dynamics section.

B. Molecular Dynamics Simulations. We performed BOMD simulations for 1 ns at 300 and 1000 K for both isomers. During the simulation, the total energy was maintained within 0.5 kJ/mol. In no case any topological rearrangement, i.e., a rotation or flipping process of the encapsulated molecule, has been observed. Using the Eyring equation, one transition within our simulation would correspond to ≈90 kJ/mol. As we do not observe any rearrangement, the transition barrier is expected to be much higher for both isomers. Indeed, explicit scanning of the rotation of the Sc_3N cluster in $Sc_3N@C_{68}$:6140 with reoptimization of the cage gives an estimate of a barrier of 356 kJ/mol at the PBE/DZVP level. Thus, the dynamical behavior of $Sc_3N@C_{68}$ is qualitatively different from Sc_3NC_{80}, where the Sc_3N unit is tumbling and rotating at ambient conditions already at the ps time scale. In detail, the carbon atoms of the cages show the typical oscillations, and the Sc atoms of the encapsulated cluster are always coordinated to the same pentalene unit, where it is sitting on top of the pentagon hinge. The MD simulations also explain the strong symmetry breaking of the X-ray spectrum. The Sc atoms are strongly coordinated to the pentalene units. This is supported by the—at the DFTB level—slightly shorter average Sc−N bond lengths compared to $Sc_3N@C_{80}$. On the other hand, the N oscillates in the cage center. The observed X-ray ScNSc angles are in the typical range of what we find in several snapshot geometries of our MD simulations and hence existing geometries on the femtosecond−picosecond time scale. A typical instantaneous structure is given in Figure 3. On the other hand, the time-average of the ScNSc angles during the full MD is 119.2 ± 0.9° for the $Sc_3N@C_{68}$:6140 isomer. In conclusion, the symmetry breaking of the X-ray geometry is similar to individual instantaneous structures, while the optimized structure corresponds to the long-time average. Therefore, the comparison of X-ray and optimized geometries alone is not a striking criterion for the assignment of isomer structures − at least for endohedral fullerenes.

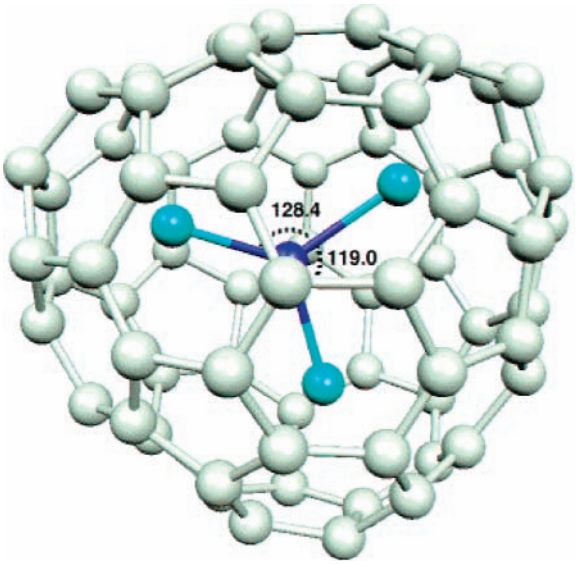

Figure 3. Typical snapshot of a DFTB BOMD trajectory of $Sc_3N@C_{68}$:6140. ScNSc angles are indicated.

C. Simulation of the ^{13}C NMR Pattern. In Figure 4, we compare the ^{13}C NMR spectrum of the two isomers of $Sc_3N@C_{68}$ with the idealized experimental structure of ref 2. The corresponding chemical shifts are given in Tables 3 and 4. The symmetry of the fully optimized structures are subject to some numerical noise, and so are the computed chemical shifts. Therefore, we have calculated ^{13}C NMR chemical shifts for all atoms of both cages and afterward averaged those nuclei which are symmetrically equivalent. The rms errors due to this averaging are also given in Tables 3 and 4. For both isomers, the rms error of the averaging is below 0.25 ppm, and hence far below the intrinsic inaccuracy of the ^{13}C NMR computation of a fullerene.[16] When the full-intensity signals are compared, the calculation of $Sc_3N@C_{68}$:6140 shows a very similar pattern

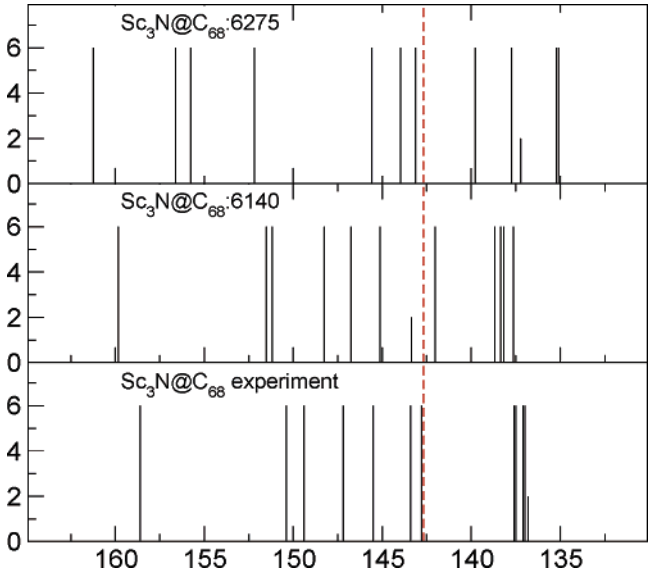

Figure 4. Comparison of ^{13}C NMR pattern of $Sc_3N@C_{68}$ isomers 6140 (middle) and 6275 (top) with experiment. Intensities are given in atoms per cage. The dashed red line denotes the C_{60} signal.

TABLE 3: Computed ^{13}C NMR Chemical Shifts for $Sc_3N@C_{68}$:6140[a]

label	intensity	δ_{TMS}	rms
C01	6	159.84	0.0803
C02	6	151.51	0.1718
C03	6	151.18	0.1327
C04	6	148.27	0.1012
C05	6	146.75	0.0889
C06	6	145.11	0.2521
C07	2	143.36	0.0780
C08	6	142.03	0.0962
C09	6	138.67	0.1174
C10	6	138.34	0.0635
C11	6	138.16	0.1296
C12	6	137.63	0.0448

[a] The atoms are labeled as given in Figure 5. The intensities (atoms per cage), ^{13}C NMR chemical shifts with respect to TMS (δ_{TMS} in ppm), and rms errors of computed signals (in ppm) are given.

as experiment. The overall spectrum is shifted systematically by 1.2 ppm to lower fields. A single, low-field signal is found experimentally at ~158.6 ppm, and calculated at 159.8 ppm. The next signal at higher fields is found experimentally at 150.4 ppm, i.e., 8.2 ppm higher. In our computation this difference is

TABLE 4: Computed ^{13}C NMR Chemical Shifts for $Sc_3N@C_{68}$:6275[a]

label	intensity	δ_{TMS}	rms
C01	6	161.24	0.0487
C02	6	156.61	0.0784
C03	6	155.77	0.1245
C04	6	152.18	0.1295
C05	6	145.59	0.0610
C06	6	143.97	0.0755
C07	6	143.13	0.1042
C08	6	139.77	0.0608
C09	6	137.74	0.0733
C10	2	137.21	0.0205
C11	6	135.22	0.1088
C12	6	135.09	0.0198

[a] Details as in Table 3.

8.3 ppm. The forthcoming five high-intensity signals are almost equally distributed, and therefore, experiment and simulation cannot be compared line by line. However, the last line is in close vicinity to the C_{60} signal. At the high-field end of the ^{13}C NMR pattern a cluster of four lines can be found, both in experiment and simulation. This gives an overall width of the high-intensity signals of 22.21 ppm in simulation compared to 21.6 ppm in experiment. In summary, calculated and measured high-intensity signals are in excellent agreement. In contrast, the single low-intensity peak is at a completely different position, marking the high-field signal for experiment (136.8 ppm), but our simulation finds its position close to the C_{60} signal at 143.4 ppm. The difference between calculated and measured signals is 6.6 ppm, and hence beyond the accuracy of our simulations. The simulated ^{13}C NMR pattern of isomer $Sc_3N@C_{68}$:6275, on the other hand, differs quite strongly from the experimental one. Its overall range is much wider than found in experiment (26.15 ppm). The two most characteristic features, the clustered four signals at the high-field end and the big gap between the first and second low-field signals are not present in the simulation. On the other hand, the low-intensity signal matches that of experiment rather closely at 137.2 ppm (simulation) vs 136.8 ppm.

The overall agreement of $Sc_3N@C_{68}$:6140 with experiment is much better than for $Sc_3N@C_{68}$:6275. Moreover, the ground-state assignment of $Sc_3N@C_{68}$ to isomer 6140 is also supported by the closer geometry agreement to experiment and the lower energy of $Sc_3N@C_{68}$:6140. However, the low-intensity signal cannot be confirmed by our computation. As the signal corresponds to the two carbons located at north and south poles

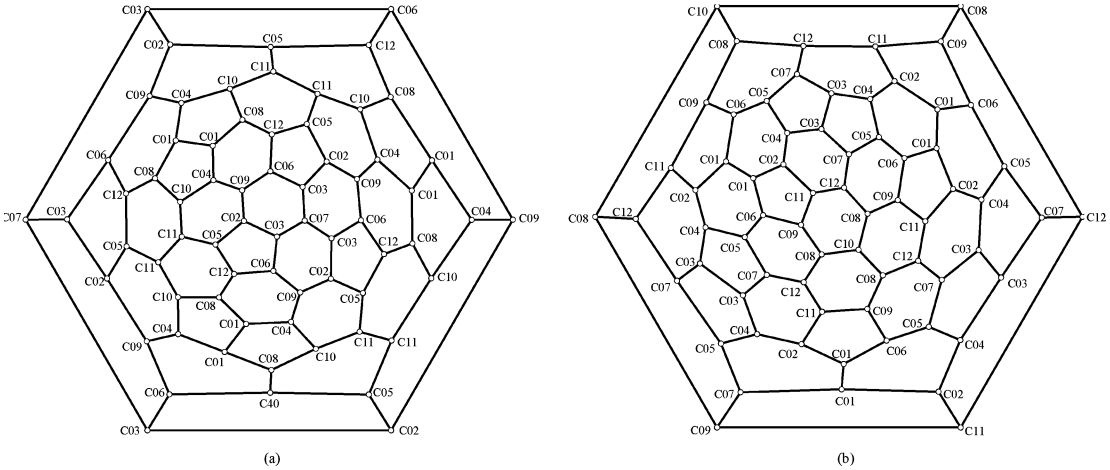

Figure 5. Schlegel diagrams of $Sc_3N@C_{68}$:6140 (a) and $Sc_3N@C_{68}$:6275 (b). Atomic labels respect the cage symmetries and are given to assign computed ^{13}C NMR signals of Tables 3 and 4.

of the cage, the signal might be influenced by oscillations of the encapsulated cluster, in particular of the N atom, along the C_3 axis. To exclude such an unlikely dynamical effect we computed the dynamically averaged ^{13}C NMR signals. We took 250 individual snapshots (each 1 ps) from a DFTB MD trajectory, which has been equilibrated to have an average temperature of 300 K, and which was running in a microcanonic NVE ensemble. ^{13}C NMR computations have been performed at a slightly lower computational level as for the static computations. We used the same computational method as for the static DFT-NMR calculations except that we employed the IGLO-II basis instead of IGLO-III.[28] For each carbon atom of the cage the ^{13}C NMR peak was computed by averaging the signals of all 250 snapshots. This procedure has been applied recently to $Sc_3N@C_{80}$[15] for which computed and measured ^{13}C NMR chemical shifts differ by only 2 ppm. For $Sc_3N@C_{68}$, the trajectories are not long enough to achieve resolution which can distinguish between the clustered high-intensity signals of $Sc_3N@C_{68}$:6140. However, the simulation finds the low-intensity peak at slightly lower fields than the C_{60} signal, confirming the signal obtained from the static calculation. Given the low signal-to-noise ratio in experiment,[2] our calculations suggest that the low-intensity line has been misassigned in experiment. The assigned signal is probably due to impurities or noise, and the calculated ^{13}C NMR data predict the low-intensity line at slightly lower fields than the signal of C_{60}. Finally, we assigned our simulated signals to the cage atoms in Figure 5.

IV. Conclusion

We showed that $Sc_3N@C_{68}$ can be assigned to the isomer $Sc_3N@C_{68}$:6140 on grounds of relative energy, geometrical data and ^{13}C NMR pattern from first principle calculations. $Sc_3N@C_{68}$:6140 is an endohedral fullerene where each Sc atom is coordinated to equatorial pentagon−pentagon bonds of pentalene units. The Sc atoms are attached strongly to the pentalenes, while the N atom oscillates in the cage center with amplitudes which explain the symmetry break observed in a recent X-ray study. The simulated ^{13}C NMR pattern of the static, optimized structure of $Sc_3N@C_{68}$:6140 is in close agreement with experiment except for the low-intensity signal, which has been probably misassigned. This result confirms that the optimized $Sc_3N@C_{68}$ geometry is close to the averaged geometry over the time scale of the ^{13}C NMR experiment. Encapsulated Sc_3N stabilizes C_{68} locally at the pentalene units and leads to a topological structure which is stable at the ns time scale, even at 1000 K. This is in contrast to $Sc_3N@C_{80}$, where the endohedral molecule rotates and tumbles on the picosecond time scale.

Acknowledgment. Financial support from CONACyT (Ph.D. Grant 154871 for J.U.R., research Projects 36037-E and 40379-F) is gratefully acknowledged. T.H. gratefully acknowledges financial support of the Deutsche Forschungsgemeinschaft (DFG).

References and Notes

(1) Stevenson, S.; Rice, G.; Glass, T.; Harich, K.; Cromer, F.; Jordan, M. R.; Craft, J.; Hadju, E.; Bible, R.; Olmstead, M. M.; Maitra, K.; Fisher, A. J.; Balch, A. L.; Dorn, H. C. *Nature (London)* **1999**, *401*, 55−57, *Nature (London)* **1999**, *402*, 898−898.

(2) Stevenson, S.; Fowler, P. W.; Heine, T.; Duchamp, J. C.; Rice, G.; Glass, T.; Harich, K.; Hajdu, E.; Bible, R.; Dorn, H. C. *Nature (London)* **2000**, *408*, 427−428.

(3) Olmstead, M. M.; de Bettencourt-Dias, A.; Duchamp, J. C.; Stevenson, S.; Marciu, D.; Dorn, H. C.; Balch, A. L. *Angew. Chem., Int. Ed.* **2001**, *40*, 1223−1225.

(4) Duchamp, J. C.; Demortier, A.; Fletcher, K. R.; Dorn, D.; Iezzi, E. B.; Glass, T.; Dorn, H. C. *Chem. Phys. Lett.* **2003**, *375*, 655−659.

(5) Olmstead, M. M.; Lee, H. M.; Duchamp, J. C.; Stevenson, S.; Marciu, D.; Dorn, H. C.; Balch, A. L. *Angew. Chem., Int. Ed.* **2003**, *42*, 900−903.

(6) Alvarez, L.; Pichler, T.; Georgi, P.; Schwieger, T.; Peisert, H.; Dunsch, L.; Hu, Z.; Knupfer, M.; Fink, J.; Bressler, P.; Mast, M.; Golden, M. S. *Phys. Rev. B* **2002**, *66*, 035197.

(7) Krause, M.; Kuzmany, H.; Georgi, P.; Dunsch, L.; Vietze, K.; Seifert, G. *J. Chem. Phys.* **2001**, *115*, 6596−6605.

(8) Dunsch, L.; Krause, M.; Noack, J.; Georgi, P. *J. Phys. Chem. Solution* **2004**, *65*, 309−315.

(9) Iezzi, E. B.; Cromer, F.; Stevenson, P.; Dorn, H. C. *Synth. Met.* **2002**, *128*, 289−291.

(10) Lee, H. M.; Olmstead, M. M.; Iezzi, E.; Duchamp, J. C.; Dorn, H. C.; Balch, A. L. *J. Am. Chem. Soc.* **2002**, *124*, 3494−3495.

(11) Kobayashi, K.; Sano, Y.; Nagase, S. *J. Comput. Chem.* **2001**, *22*, 1353−1358.

(12) Aihara, J. *J. Phys. Chem. A* **2002**, *106*, 11371−11374.

(13) Aihara, J. *Chem. Phys. Lett.* **2001**, *343*, 465−469.

(14) Larade, B.; Taylor, J.; Zheng, Q. R.; Mehrez, H.; Pomorski, P.; Guo, H. *Phys. Rev. B.* **2001**, *64*, 195402.

(15) Heine, T.; Vietze, K.; Seifert, G. *Magn. Reson. Chem.* **2004**, *42*, 199−201.

(16) Heine, T. Fullerenes. In *Calculation of NMR and EPR Parameters: Theory and Applications*; Kaupp, M., Malkin, V. G., Bühl, M., Eds.; Wiley-VCH: Weinheim, Germany, 2004.

(17) Campanera, J. M.; Bo, C.; Olmstead, M. M.; Balch, A. L.; Poblet, J. M.; *J. Phys. Chem. A* **2002**, *106*, 12356.

(18) Albertazzi, E.; Domene, C.; Fowler, P. W.; Heine, T.; Seifert, G.; Van Alsenoy, C.; Zerbetto, F. *Phys. Chem. Chem. Phys.* **1999**, *1*, 2913−2918.

(19) Fowler, P. W.; Manolopoulos, D. E. *An Atlas of Fullerenes*; Clarendon Press: Oxford, U.K., 1996.

(20) Katz, T. J.; Rosenberger, M. *J. Am. Chem. Soc.* **1962**, *84*, 865−866.

(21) Köster, A. M.; Calaminici, P.; Flores-Moreno, R.; Geudtner. G.; Goursot, A.; Heine, T.; Janetzko, F.; Reveles, J. U.; Vela, A.; Patchkovskii, S.; Salahub, D. R. *deMon2k*; NRC: Ottawa, Canada 2003. http://www.de-Mon-software.com.

(22) Malkin, V. G.; Malkina, O. L.; Salahub, D. R. *deMon-NMR 1.0*: NRC: Ottawa, Canada, 2002.

(23) Auxiliary functions have been generated automatically at the GEN-A2 level (including s, p, and d functions) for C and at the GEN-A2* level (including s, p, d, f, and g functions) for Sc and, N. See: Köster, A. M.; Calaminici, R.; Gómez, Z.; Reveles, J. U. In *Reviews of Modern Quantum Chemistry*; Sen, K. D., Ed.; World Scientific Publishing: Singapore, 2002; Volume II.

(24) Köster, A. M.; Reveles, J. U.; M. del Campo, J. *J. Chem. Phys.* **2004**, *121*, 3417−3424.

(25) Köster, A. M.; Flores-Moreno, R.; Reveles, J. U. *J. Chem. Phys.* **2004**, *121*, 681−690.

(26) Perdew, J. P.; Burke, K.; Ernzerhof, M. *Phys. Rev. Lett.* **1996**, *77*, 3865−3868.

(27) Godbout, N.; Salahub, D. R.; Andzelm, J.; Wimmer, E. *Can. J. Chem.* **1992**, *70*, 560−571.

(28) Kutzelnigg, W.; Fleischer, U.; Schindler, M. In *NMR−Basic Principles and Progress*; Springer-Verlag: Heidelberg, Germany, 1990; pp 23−165.

(29) Porezag, D.; Frauenheim, T.; Köhler, T.; Seifert, G.; Kaschner, R. *Phys. Rev. B* **1995**, *51*, 12947−12957.

(30) Reveles, J. U.; Köster, A. M. *J. Comput. Chem.* **2004**, *25*, 1109−1116.

(31) Taylor, R.; Hare, J. P.; Abdul-Sada, A. K.; Kroto, H. W. *J. Chem. Soc., Chem. Commun.* **1990**, 1423−1425.

(32) Kroto, H. W. *Nature (London)* **1987**, *329*, 529−531.

(33) Schmalz, T. G.; Seitz, W. A.; Klein, D. J.; Hite, G. E. *J. Am. Chem. Soc.* **1988**, *110*, 1113−1127.

(34) Fowler, P. W.; Heine, T.; Zerbetto, F. *J. Phys. Chem. A* **2000**, *104*, 9625.

(35) It is quite likely that other $Sc_3N@C_{68}$ isomers out of the 6332 possibilities are more stable than $Sc_3N@C_{68}$:6275, but they are not compatible with the observed ^{13}C NMR pattern.